Materials and Methods

Animals and Surgical Procedures

All experimental procedures were performed in accordance with the National Institutes of Health Guide for the Care and Use of Laboratory Animals and were approved by the Indiana University Bloomington IACUC. A total of 24 male mice (14 PV-Cre and 10 wild-type) were used. Adult male C57BL/6 mice (8–12 weeks; The Jackson Laboratory) or PV-Cre mice (RRID:IMSR_JAX:017320) were single-housed after surgery on a 12-h light/dark cycle with ad libitum food and water.

For awake head-fixed recordings, mice were anesthetized with isoflurane (1–2% in O_2) and implanted with a custom headplate (Luigs & Neumann GmbH, Ratingen, Germany). For optogenetic experiments in PV-Cre mice, AAV5-CAG-FLEX-ArchT-tdTomato (gift from Edward Boyden, Addgene viral prep # 28305-AAV5; http://n2t.net/addgene:28305; RRID:Addgene_28305) was injected (100 nL per depth) into the right AStria (AP: -1.7, ML: +4.0, DV: -3.0 mm from bregma, at a 10° angle) and LA (AP: -1.7, ML: +4.0, DV: -3.6 mm from bregma, at a 10° angle). A fiber optic cannula (400 µm diameter; Thorlabs GmbH, Bergkirchen, Germany) was implanted (AP: -1.7, ML: +2.5, DV: -3.5 mm at a 10° angle). Implants were secured with dental cement. Mice received carprofen (5 mg/kg, s.c.) and recovered for 7–10 days while being habituated to head-fixation.

Electrophysiology and Optogenetics

Acute silicon probes (P1/H15, 64/128-ch; Cambridge Neurotech) were coated with DiI (Thermo Fisher) for visualize the probe track and inserted into the right amygdala of awake, head-fixed mice. Signals were acquired at 30 kHz (Intan RHD2000), filtered (0.3–6 kHz), and sorted with Kilosort2.5 (REF). Clusters were manually curated in Phy (REF). Clusters with refractory period violations >0.5% were excluded. Only neurons with stable firing rates across the recording session were included in the analysis. Units were classified as putative principal neurons (PNs; trough-to-peak > 0.4 ms) or interneurons (INs; trough-to-peak < 0.4 ms, firing rate > 10 Hz).

Auditory (2.8 kHz tone, 70 dB, 50 ms) and tail shock (0.7 mA, 10 ms) stimuli were delivered pseudorandomly (50-100 trials/condition, 5-10 s ITI) using custom MATLAB/Arduino software. For optogenetic inhibition, a 635 nm laser (10 mW/mm², CNI Laser) was delivered through the cannula to activate ArchT in PV neurons, with light-on/off trials interleaved.

Data Analysis and Statistics

Analyses were performed with custom MATLAB scripts (R2024b). Peristimulus histograms (PSTHs, 1 ms bins, -5 to +4 s from stimulus) were smoothed with a Savitzky-

Golay filter (201 ms for population, 5 ms for monosynaptic analysis) and delay-corrected. Baselines were from -5 to 0 s.

The burst index (adapted from Royer et al., 2012) was calculated using the CellExplorer framework (REF). To quantify bursting propensity, we computed the ratio of the mean autocorrelogram (ACG) value (3–5 ms) to the baseline (mean of 200–300 ms). Values > 1 indicate a higher probability of short-interval spikes (bursts) relative to tonic firing.

Neuronal Classification: Neurons were classified based on z-scored responses. For population analysis (Figs 2, 3), excitation was $z \geq 2$ (0-1s window) and inhibition was a ≥50% firing rate drop. For monosynaptic analysis (Fig. 4), $z \geq 5$ and probability ≥ 0.1 was used. The initial 10 ms post-US were excluded. Functionally, neurons were clustered as CS-selective, US-selective, Multisensory, Non-responsive, or Inhibited.

Statistical Comparisons: Proportions were compared using Chi-square test with Cramér's V effect size. Non-normal distributions (firing rates, latencies, durations) were compared using Wilcoxon rank-sum tests (for two groups) or Kruskal-Wallis ANOVA (for three or more groups) followed by Dunn's post-hoc test. Repeated measures (e.g., CS vs. US vs. CS+US responses) were analyzed using Friedman ANOVA with post-hoc Wilcoxon signed-rank test. For optogenetics, light-on/off trials were compared using a Wilcoxon signed-rank test or paired t-test. Data are reported as mean ± SEM, except for baseline spike feature characterizations which are mean ± SD. Statistical significance was defined as $p < 0.05$.

Immunohistochemistry and imaging

To verify viral expression and electrode placement, mice were anesthetized with isoflurane after the recordings and decapitated. Brains were removed, post-fixed for 24 hours in 4% paraformaldehyde (PFA), and sectioned coronally (50 µm) on a Leica VT1200S vibratome. Immunostaining was used to verify the specificity of ArchT expression in PV interneurons. Sections were blocked using 10% Normal Donkey Serum in 0.5% Triton X-100 dissolved in 0.1 M PB and incubated for 4 days at 4°C with primary antibody (guinea pig anti-PV, 1:10,000; Synaptic Systems, 195 004). Sections were then incubated with secondary antibody (donkey anti-guinea pig Alexa 488, 1:1000; Jackson ImmunoResearch, 706-545-148) overnight at room temperature. Images were acquired using a confocal microscope (Leica VT1000S) to confirm overlap between ArchT-tdTomato expression and PV immunolabeling.

Commented [NH1]: Was anti-RFP used to enhanced tdT signals?

Histology and code accessibility

Probe placement was confirmed histologically on 150 µm coronal sections using DiI tracks. Only data from on-target animals were included. Analysis scripts are available from the corresponding author upon reasonable request.

Results

Similar firing dynamics in LA and AStria characterize CS- and US-evoked responses

To reveal the spike responses in amygdala circuits during stimulus processing, we recorded single-unit activity from 24 mice across four subregions: the lateral amygdala (LA, n = 293), basal amygdala (BA, n = 219), amygdalostriatal transition area (AStria, n = 120), and central amygdala (CeA, n = 50) in awake, head-fixed mice (Figure 1A). Electrode placement was reconstructed post hoc by visualizing the silicon probe tracks using DiI, confirming targeting of the LA, BA, AStria, and CeA (Figure S1A-E). In the LA and BA, units were classified as putative principal neurons (PNs) or putative fast-spiking interneurons (INs) based on spike waveform features and autocorrelograms (Figure 1C, D). PNs exhibited significantly longer spike trough-to-peak durations and lower firing rates compared to INs (Table 1). In the CeA and AStria, local inhibitory cells could not be separated from medium spiny neurons based on these two spiking features, therefore, all units were pooled together. Overall, our baseline characterization of firing across these four subregions revealed that CeA neurons showed the lowest spike rates and bursting properties (Figure 1E, F; Table 1). Lastly, we inspected the response stability during the experiments by analyzing the changes in firing rates across blocks and confirmed consistent activity levels throughout the recording sessions (Supplementary Figure 2; Table 2).

The canonical model of the amygdala posits that the LA and BA function as a tightly coupled unit, where sensory information integrated in the LA is relayed to the BA before transmission to output nuclei like the CeA (Johansen 2011). We tested this hypothesis by comparing subregional responses to the conditioned stimulus (CS; tone) and unconditioned stimulus (US; shock) (Figure 1B). We classified neurons into distinct functional types: CS-selective, US-selective, Multisensory, Non-responsive, or Inhibited (Figure 2A, B). In the LA, we observed a diverse distribution of responsiveness: CS-selective (12%, n = 34), US-selective (18%, n = 53), Multisensory (24%, n = 69), Non-responsive (22%, n = 63), and Inhibited (25%, n = 74). This profile was strikingly mirrored in the AStria, which showed a similar composition: CS-selective (10%, n = 12), US-selective (16%, n = 19), Multisensory (28%, n = 34), Non-responsive (23%, n = 28), and Inhibited (23%, n = 27). In contrast, the BA was dominated by Non-responsive (40%, n = 88) and Inhibited (38%, n = 83) neurons, with a smaller US-selective population (17%, n = 37) and a minority of Multisensory units (5%, n = 11). Similarly, the CeA was largely quiescent, primarily comprised of Non-responsive (50%, n = 25) and Inhibited (38%, n = 19) cells, with smaller populations of US-selective (8%, n = 4) and Multisensory (4%, n = 2) neurons. These data reveal a dissociation between the LA and BA in sensory stimulus processing, while highlighting that the AStria can be a parallel processing partner to the LA.

To strengthen this conclusion, we compared the proportions of the five response categories among the four regions. We found that the LA and AStria exhibited statistically indistinguishable distributions (Chi-square test, $p = 0.805$, Cramér's $V = 0.06$; Figure 2B). In contrast, both the BA and CeA showed significantly lower responsiveness that was comparable in these two nuclei (Chi-square test, $p < 0.001$, Cramér's $V = 0.23$; Figure 2C). As US evoked spiking in a similar ratio of neurons in the LA, BA and AStria, we wondered whether the response properties of US-excited neurons were similar in these regions. We found that US-driven activity was robust and matched across LA, AStria, and BA, whereas responses in the BA were significantly shorter in duration (Figure 2D, Table 3). These findings further suggest that, under these conditions, the LA and AStria - not the LA and BA - operate as the primary functional unit for processing sensory stimuli.

LA and AStria form a parallel integration module

If the LA and AStria function as a unified processing node, they should integrate sensory information similarly. We tested this by analyzing responses to simultaneous CS and US presentation in the responsive clusters of both regions (Figure 3A-D). CS-selective neurons exhibited significant response suppression during combined stimulation in both regions (Figure 3 E-F, Table 4). US-selective neurons maintained robust firing, with AStria responses showing no significant change and LA responses showing only a slight reduction. In Multisensory neurons, we found no evidence of supralinear summation. In the LA, the combined response significantly exceeded individual responses. In the AStria, while the overall Friedman test was significant, post-hoc comparisons did not reveal significant differences between conditions. To confirm the robustness of our functional classifications, we performed a parallel analysis restricted to principal neurons (PNs) in the LA, which largely recapitulated the identified response clusters (Figure S3A-E, Table 5). Crucially, a direct comparison of response magnitudes (i.e., the firing rate, FR) across all responsive neurons confirmed that signal gain was identical across the LA and AStria for CS, US, and combined stimuli (Table 6) (Figure 3G). These gain dynamics were observed alongside similar proportions of responsive cell types (Chi-square test, $\chi^2 = 1.20$, $p = 0.555$, Cramér's $V = 0.07$; Figure 3H), supporting the hypothesis of shared integration properties.

Parallel monosynaptic drive to the LA-AStria unit

The synchronization of LA and AStria activity driven by CS and US raises the question of their afferent connectivity. As previous studies showed that the inputs from the thalamus innervate both the LA and AStria (REF), we analyzed onset latencies of spikes to identify monosynaptic responses ($\leq$25 ms) indicative of direct subcortical drive (Figure 4A, C). We identified a significant population of neurons that emitted short-latency spikes in both regions. Mirroring the large time scale dynamics, monosynaptic integration varied by cell type (Figure 4B, D). While CS-selective neurons exhibited profound suppression during combined stimulation (Table 7), US-selective neurons maintained elevated firing. In

Multisensory neurons, the combined monosynaptic response was driven by the US magnitude without supralinear summation. The magnitude of these monosynaptic responses was comparable across stimuli in both nuclei (Table 8; Figure 4B, D, F; Figure S5E). Whereas the onset latencies for US responses were statistically indistinguishable between regions, CS responses were significantly faster in the AStria compared to the LA (Figure 4G). This timing, with AStria responding prior to or concurrently with the LA, rules out a simple serial relay from LA to AStria at short-latency spiking.

Shared inhibitory control mechanisms

Finally, we asked whether this functional similarity extends to local circuit regulation. Parvalbumin (PV)-expressing interneurons provide powerful feedforward inhibition in the LA (REFS). To determine if this mechanism is conserved in the AStria, we targeted PV interneurons in PV-Cre mice (N = 12) by injecting a Cre-dependent inhibitory opsin (AAV5-CAG-FLEX-ArchT-tdTomato) into the amygdala (Figure 5A). Immunohistochemical analysis confirmed specific expression of ArchT in PV interneurons in both the LA and AStria (Figure 5B). To reveal the function of PV interneurons in controlling short-latency spiking, we optogenetically silenced these inhibitory cells during stimulus presentation. First, we confirmed the efficacy of PV interneuron silencing by analyzing their baseline firing rates during the pre-stimulus laser illumination period (-0.5s to 0s). In light-inhibited neurons (LA: n=16, AStria: n=6), laser illumination significantly suppressed baseline firing rates in both regions (LA: 4.59 ± 0.91 Hz no-light vs 1.69 ± 0.38 Hz light, $p < 0.001$; AStria: 5.69 ± 0.93 Hz no-light vs 2.02 ± 0.33 Hz light, $p < 0.001$; Wilcoxon signed-rank test; Figure S4A-E). This corresponded to a mean firing rate reduction of 63.20% in LA neurons and 64.50% in AStria neurons. Then, we assessed the effect of inhibition of PV interneurons on CS- and US-triggered spiking., We found that inhibiting PV interneurons resulted in modulated sensory responses in single neurons from both the LA and AStria (Figure 5C, D). We observed distinct subpopulations that either increased or decreased their firing rates. The proportion of neurons exhibiting increased, decreased, or unchanged responses was similar in LA and AStria for both CS (Chi-square test, $\chi^2 = 4.28$, $p = 0.117$) and US stimuli (Chi-square test, $\chi^2 = 3.48$, $p = 0.176$; Figure 5E). In the LA, a substantial proportion of neurons decreased their response (CS: 39%, n=11; US: 34%, n=12), exhibiting significant reductions in firing rate (Table 9, Figure 5F-G). A smaller subset showed increased activity (CS: 14%, n=4; US: 11%, n=4), with significantly elevated firing rates. In the AStria, response modulation was also bidirectional, with neurons exhibiting decreased activity (CS: 16%, n=5; US: 16%, n=5) or increased activity (CS: 19%, n=6; US: 9%, n=3). The fact that both regions operate under an identical feedforward inhibition further strengthen the hypothesis that LA-AStria work in parallel during sensory signal processing. Together, these data define the LA and AStria as a distinct, cohesive functional unit, sharing input sources, integration properties, and inhibitory control, from the downstream BA.

Table 1: Baseline characterization of firing rates and bursting properties.

Region	Cell Type	n	FR (Hz)	Burst Index	Trough-to-peak (ms)
LA	PNs	276	3.33 ± 3.35	1.40 ± 5.35	0.613 ± 0.161
LA	INs	17	16.58 ± 6.74	1.21 ± 0.91	0.316 ± 0.035
BA	PNs	196	4.39 ± 4.47	4.57 ± 10.21	0.623 ± 0.162
BA	INs	23	20.98 ± 7.94	0.71 ± 0.65	0.286 ± 0.057
AStria	All	120	4.99 ± 6.80	0.54 ± 1.17	n.d.
CeA	All	50	2.04 ± 2.96	0.44 ± 1.02	n.d.
Kruskal-Wallis Test (LA PNs, BA PNs, AStria, CeA)			χ^2=20.81, p<0.001	χ^2=38.34, p<0.001	

Values presented as Mean ± SD. n indicates number of neurons.

Table 2: Block-by-block firing rate (Hz) evolution across regions and stimuli.

Region / Stimulus	Block 1	Block 2	Block 3	Block 4	Block 5	Block 6	Block 7	Block 8	Block 9	Block 10
LA CS	16.37 ± 1.82	14.69 ± 1.57	13.16 ± 1.43	12.04 ± 1.31	11.48 ± 1.12	11.57 ± 1.09	11.29 ± 0.99	10.94 ± 1.02	10.01 ± 0.92	10.58 ± 0.91
LA US	14.48 ± 1.38	13.81 ± 1.34	13.00 ± 1.30	13.33 ± 1.28	12.88 ± 1.18	13.84 ± 1.40	13.49 ± 1.22	13.84 ± 1.32	13.28 ± 1.24	12.85 ± 1.29
BA US	13.26 ± 1.88	12.08 ± 1.72	11.95 ± 1.60	12.10 ± 1.59	11.86 ± 1.58	12.30 ± 1.60	12.10 ± 1.63	12.18 ± 1.45	11.95 ± 1.55	11.96 ± 1.58
AStria CS	13.83 ± 1.59	11.71 ± 1.11	11.25 ± 1.14	10.62 ± 1.06	9.83 ± 0.99	9.53 ± 1.05	9.36 ± 0.97	9.47 ± 1.11	8.50 ± 0.94	8.18 ± 1.00
AStria US	15.68 ± 2.19	15.75 ± 2.44	14.48 ± 1.70	14.58 ± 2.09	13.74 ± 1.73	13.40 ± 1.70	12.02 ± 1.51	12.86 ± 1.61	12.32 ± 1.45	12.29 ± 1.59

Data are presented as Mean ± SEM

Table 3: Comparison of US-evoked excitatory responses across amygdala regions.

Region	Firing Rate (Hz)	Response Duration (ms)
LA	51.55 ± 5.47	301.73 ± 23.82
AStria	50.59 ± 8.75	294.04 ± 32.96
BA	41.13 ± 5.05	119.15 ± 17.30
Kruskal-Wallis p-value	p = 0.594	p < 0.001
Dunn's Post-hoc	-	LA vs BA: p < 0.001 AStria vs BA: p < 0.001 LA vs AStria: p > 0.999

Data are presented as mean ± SEM.

Table 4: Firing rate dynamics and signal gain in LA and AStria.

Region	Cell Type / Group	Measure	CS (Hz)	US (Hz)	CS+US (Hz)	Friedman p-value	Wilcoxon Sign-rank p (CS vs. US)	Wilcoxon Sign-rank p (CS vs. CS+US)	Wilcoxon v (US vs. CS+US)
LA	CS-selective	FR	34.72 ± 4.39	7.34 ± 0.76	14.17 ± 1.98	< 0.001	< 0.001	< 0.001	< 0.001
AStria	CS-selective	FR	25.33 ± 3.58	12.18 ± 3.03	14.94 ± 3.01	< 0.001	< 0.001	< 0.001	0.129
LA	US-selective	FR	10.87 ± 1.74	31.08 ± 2.90	29.29 ± 3.11	< 0.001	< 0.001	< 0.001	0.002
AStria	US-selective	FR	14.31 ± 3.23	34.80 ± 6.21	32.45 ± 5.59	< 0.001	< 0.001	< 0.001	0.227
LA	Multisensory	FR	58.08 ± 6.53	67.28 ± 9.00	78.07 ± 10.60	< 0.001	0.189	0.002	< 0.001
AStria	Multisensory	FR	51.88 ± 9.71	59.42 ± 13.02	61.30 ± 12.24	0.026	0.135	0.033	0.118

Data are presented as mean ± SEM.

Table 5: Comparison of Principal Neuron (PN) and Interneuron (IN) responses in LA.

Functional Type	Cell Type	Measure	CS	US	CS+US
CS-selective	PN (n=34)	FR (Hz)	39.91 ± 5.33	-	13.67 ± 4.49
		Response Length (ms)	221.91 ± 29.13	-	76.41 ± 26.47
US-selective	PN (n=46)	FR (Hz)	-	29.85 ± 3.21	23.59 ± 2.92
		Response Length (ms)	-	236.70 ± 28.43	166.07 ± 23.09
	IN (n=4)	FR (Hz)	-	50.92 ± 5.67	52.82 ± 6.18
		Response Length (ms)	-	126.25 ± 48.64	189.50 ± 70.08
Multisensory	PN (n=44)	FR (Hz)	43.46 ± 6.47	40.36 ± 5.25	49.18 ± 9.47
		Response Length (ms)	205.66 ± 31.92	222.30 ± 28.82	289.36 ± 35.12
	IN (n=7)	FR (Hz)	80.06 ± 20.55	149.80 ± 61.31	178.11 ± 61.97
		Response Length (ms)	298.57 ± 127.24	346.86 ± 120.75	553.14 ± 115.50

Data presented as Mean ± SEM.

Table 6: Comparison of signal gain (firing rate) between LA and AStria across stimulus conditions.

Stimulus Condition	LA Firing Rate (Hz)	AStria Firing Rate (Hz)	Wilcoxon Rank-sum p
CS	50.37 ± 4.72	44.95 ± 7.42	0.763
US	51.55 ± 5.47	50.59 ± 8.75	0.934
Combined (CS+US)	47.57 ± 5.29	44.31 ± 6.98	0.672

Data are presented as mean ± SEM..

Table 7: Monosynaptic firing rate responses (0-25ms) in LA and AStria.

Region	Cell Type / Group	Measure	CS (Hz)	US (Hz)	CS+US (Hz)	Friedman Test (p-value)	Wilcoxon Sign-rank p (CS vs. US)	Wilcoxon Sign-rank p (CS vs. CS+US)	Wilcoxon Sign-rank p (US vs. CS+US)
LA	CS-selective	FR	21.89 ±	4.10 ± 1.22	3.19 ± 0.67	< 0.001	< 0.001	< 0.001	0.531

			4.75						
AStria	CS-selective	FR	23.12 ± 5.76	7.26 ± 2.22	6.85 ± 1.89	0.015	0.004	0.055	0.664
LA	US-selective	FR	4.96 ± 0.84	18.52 ± 2.04	16.87 ± 1.87	< 0.001	< 0.001	< 0.001	0.091
AStria	US-selective	FR	8.76 ± 2.14	34.02 ± 8.76	28.54 ± 6.39	< 0.001	< 0.001	0.001	0.076
LA	Multisensory	FR	40.59 ± 6.23	54.20 ± 7.53	55.60 ± 7.66	< 0.001	0.004	0.002	0.145
AStria	Multisensory	FR	49.51 ± 13.03	45.75 ± 12.32	43.70 ± 12.72	0.636	-		

Data are presented as mean ± SEM.

Table 8: Comparison of monosynaptic response magnitude and onset latency between LA and AStria.

Metric	Stimulus	LA	AStria	Wilcoxon Rank-sum p
Firing Rate (Hz)	CS	33.49 ± 4.40	42.91 ± 10.01	0.494
	US	34.38 ± 4.03	41.22 ± 8.25	0.523
	CS+US	27.48 ± 3.49	32.58 ± 6.99	0.322
Onset Latency (ms)	CS	16.79 ± 0.39	14.42 ± 0.61	< 0.001
	US	17.47 ± 0.30	16.66 ± 0.40	0.103

Data are presented as mean ± SEM.

Table 9: Modulation of Firing Rates by PV Interneuron Inhibition

Region	Stimulus	Response Type	n	No Light FR (Hz)	Light FR (Hz)	Statistical Test	p-value
LA	CS	Decreased	11	24.69 ± 7.41	16.31 ± 6.58	paired t-test	< 0.001
LA	US	Decreased	12	25.60 ± 6.00	16.63 ± 4.67	paired t-test	< 0.001
LA	CS	Increased	4	11.33 ± 6.55	19.61 ± 6.41	paired t-test	0.002
LA	US	Increased	4	8.88 ± 7.26	13.85 ± 7.79	paired t-test	0.004
AStria	CS	Decreased	5	47.21 ± 7.06	34.80 ± 7.12	paired t-test	0.001
AStria	US	Decreased	5	25.20 ± 6.96	16.29 ± 5.98	paired t-test	0.005
AStria	CS	Increased	6	11.51 ± 4.36	16.98 ± 4.82	paired t-test	< 0.001
AStria	US	Increased	3	20.56 ± 7.10	27.44 ± 8.57	paired t-test	0.053

Data are presented as Mean ± SEM

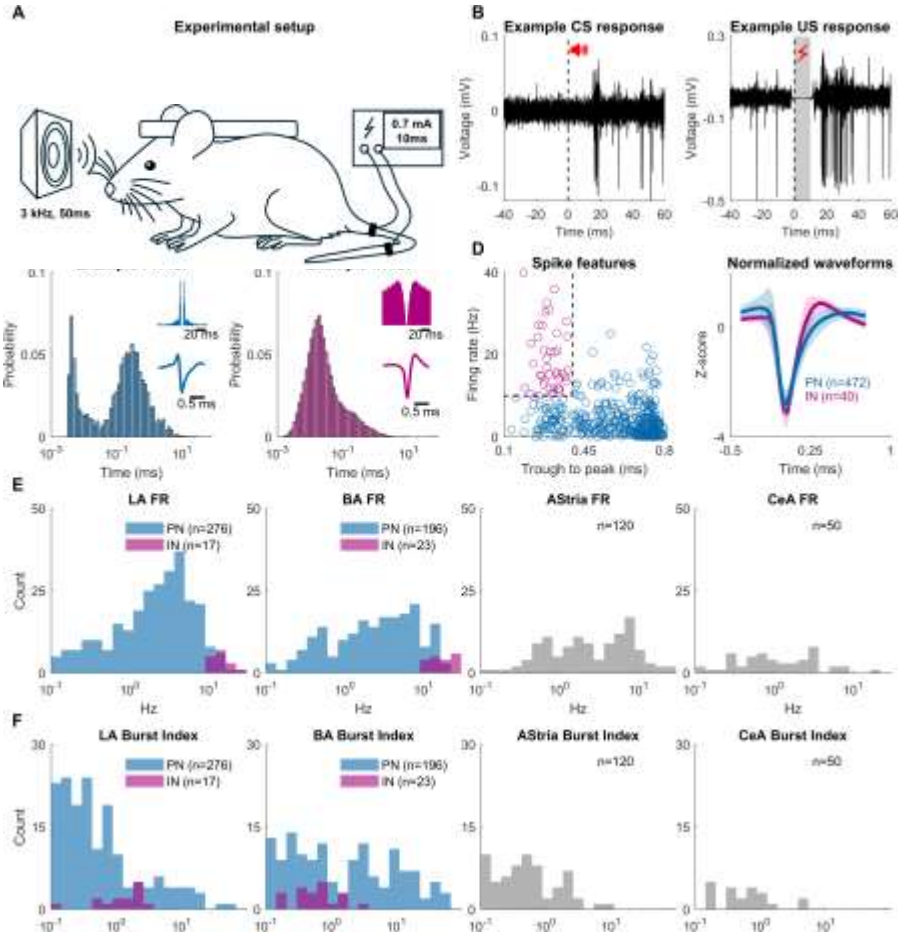

Figure 1: Characterization of neurons in the basal amygdala during fear conditioning **(A)** Experimental setup schematic showing mouse with headplate implantation, auditory conditioned stimulus (CS; 3 kHz, 50 ms tone), and unconditioned stimulus (US; 10 ms tail-shock). **(B)** Example neuronal responses to CS (left) and US (right). Top: raw voltage traces showing single-trial responses. Red signs indicate the stimulus types, dashed lines the stimulus onset (time 0), and gray shading shows the US-evoked artefact duration removed before analysis. **(C)** Example interspike interval (ISI) distributions for putative principal neurons (PN, left, blue) and fast spiking interneurons with narrow spike width (IN, right, magenta). Insets show autocorrelograms (ACG, top) with 20 ms scale bar, and average waveforms (bottom) with 0.5 ms scale bar. **(D)** Spike feature classification. Left: scatter plot of trough-to-peak time versus firing rate for LA and BA neurons. Dashed lines

indicate classification boundaries (0.4 ms and 10 Hz). Right: normalized waveforms (z-score) for PNs (blue, n=472) and INs (magenta, n=40), showing mean ± SD. **(E)** Firing rate distributions across brain regions (LA, BA, AStria, CeA). LA and BA show separate distributions for PNs (blue) and INs (magenta). Astria and CeA show combined distributions (gray). Log-spaced bins from 0.1 to 30 Hz. **(F)** Burst index distributions (Royer et al., 2012) across brain regions. Same color scheme as panel E. Log-spaced bins from 0.1 to 100.

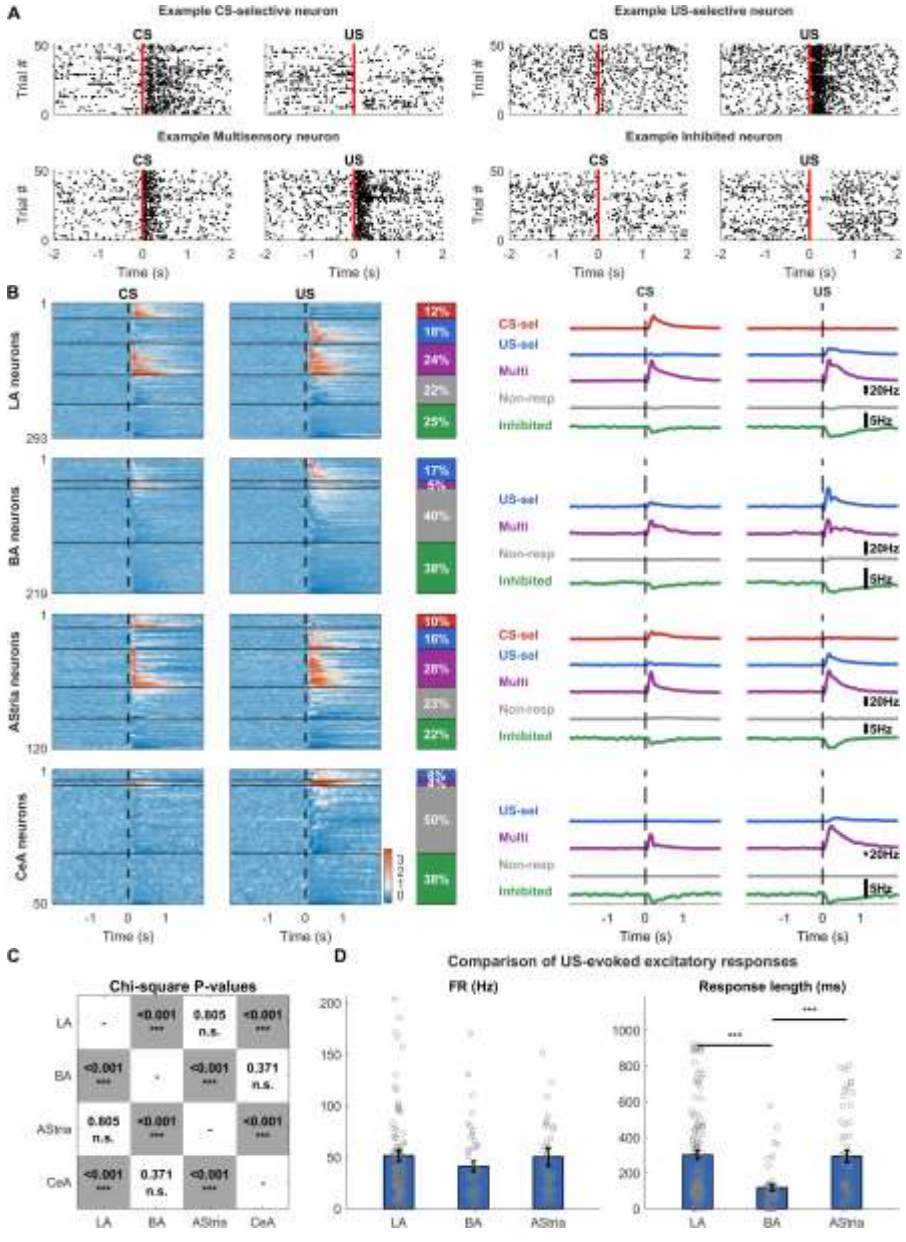
A
Example CS-selective neuron
Example US-selective neuron
Example Multisensory neuron
Example Inhibited neuron
CS
US
Trial #
Time (s)
B
LA neurons
BA neurons
AStria neurons
CeA neurons
12%
18%
24%
22%
25%
17%
5%
40%
38%
10%
16%
28%
23%
22%
8%
4%
50%
38%
CS-sel
US-sel
Multi
Non-resp
Inhibited
20Hz
5Hz
C
Chi-square P-values
LA
BA
AStria
CeA
<0.001
***
0.805
n.s.
0.371
D
Comparison of US-evoked excitatory responses
FR (Hz)
Response length (ms)

Figure 2: Regional differences in neuronal response profiles to fear conditioning stimuli.

(A) Example single-neuron raster plots for CS (left) and US (right) stimuli. Top to bottom: CS-selective neuron, US-selective neuron, Multisensory neuron, and inhibited neuron. Red vertical lines mark stimulus onset. **(B)** Population responses across four brain regions (LA, BA, AStria, CeA). Columns 1-2: Z-scored heatmaps for CS and US trials, sorted by stimulus preference. Column 3: Bar charts showing cluster proportions (CS-selective: red, US-selective: blue, Multisensory: purple, Non-responsive: gray, Inhibited: green). Columns 4-5: Average firing rate (Hz) for CS and US trials, showing mean response for each cluster with Savitzky-Golay smoothing (201 bins). **(C)** Chi-square test p-value matrix comparing cluster distributions across regions. Grayscale intensity indicates significance level: darker gray for $p<0.001$, lighter gray for $p<0.05$, white for $p\geq0.05$. Text shows exact p-values and significance markers (***$p<0.001$, **$p<0.01$, *$p<0.05$). Note the similarity between neuronal spiking in the LA and AStria. **(D)** Comparison of US-evoked excitatory response metrics across LA, BA, and AStria. Three bar graphs show the difference in firing rate (FR, Hz) and response length (ms) for US-selective and Multisensory neurons combined. Individual data points shown as circles; bars represent mean ± SEM. Statistical comparisons use Kruskal-Wallis test with post-hoc pairwise comparisons (Dunn's test).

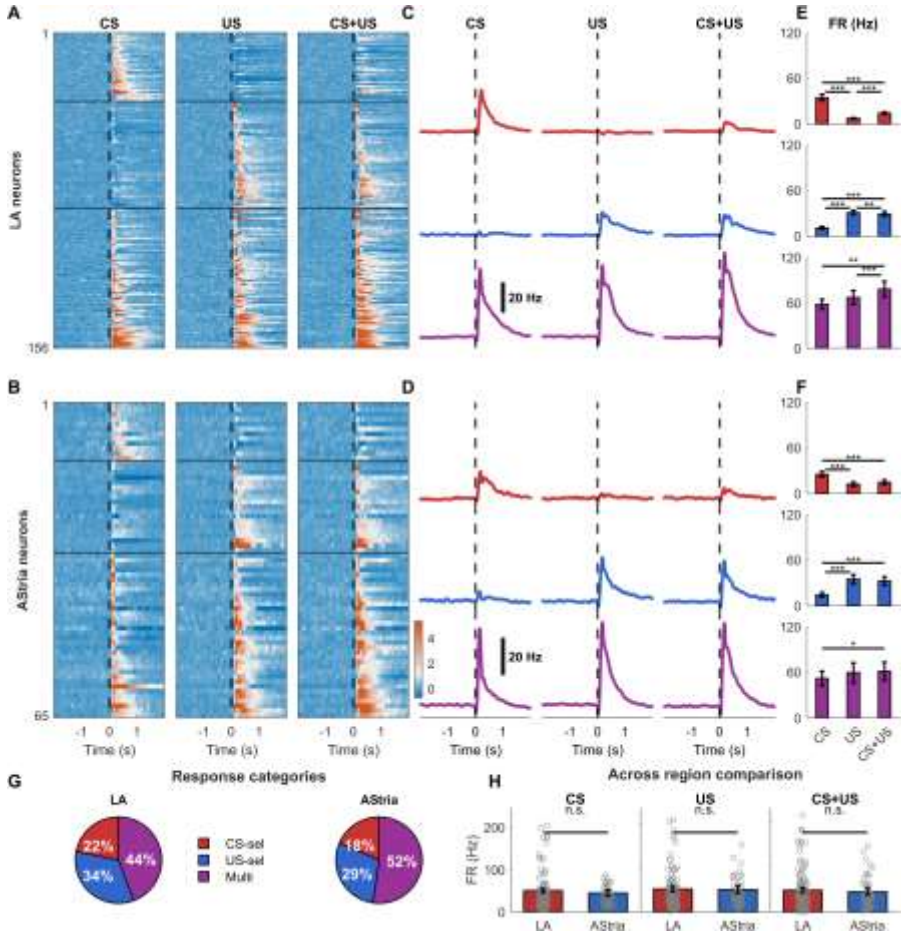

Figure 3: Similar properties of CS-selective, US-selective, and Multisensory neurons in the LA and AStria.

(A) LA heatmaps showing z-scored PSTHs for CS (left), US (middle), and CS+US (right) stimuli. Neurons sorted by cluster (CS-selective, US-selective, Multisensory) based on CS and US responses only. Color scale shows z-score normalized to baseline. Black lines separate clusters. **(B)** AStria heatmaps, same format as panel A. **(C)** Lines showing population average firing rates (Hz) for CS-selective (red), US-selective (blue), and Multisensory (purple) neurons in the LA. Each cluster displayed separately (stacked rows) for CS, US, and CS+US stimuli. Scale bar: 20 Hz. **(D)** AStria lines, same format as panel C. **(E)** LA bar charts showing firing rate (FR) comparing CS, US, and CS+US responses within each cluster. Bars show mean ± SEM. Statistical comparisons use Wilcoxon signed-

rank test ($p<0.05$, $p<0.01$, $^{**}p<0.001$). **(F)** AStria bar charts, same format as panel E. **(G)** Similar proportions of CS-selective, US-selective, and Multisensory neurons in LA (left) and Astria (right). Percentages indicate fraction of responsive neurons in each category. Legend shows cluster color coding. **(H)** Firing rate (FR) for CS (left), US (middle), and CS+US (right) responsive neurons in the LA and AStria is similar. Individual data points shown as grey circles with jitter. Bars show mean ± SEM. Statistical comparison using Wilcoxon rank-sum test ($^{*}p<0.05$, $^{**}p<0.01$, $^{***}p<0.001$, n.s.=not significant). Y-axis scaled to 95th percentile to avoid compression from outliers.

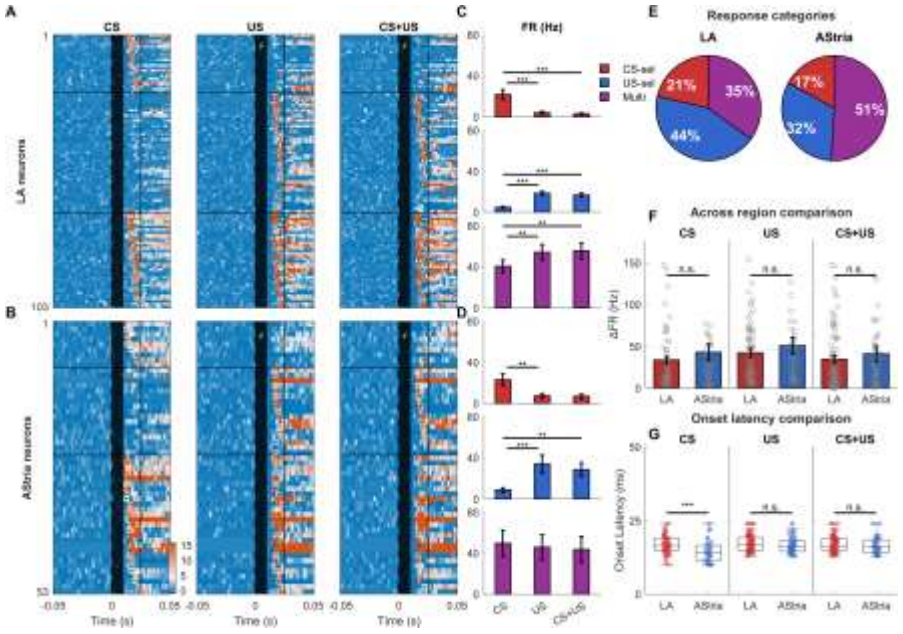

Figure 4: Monosynaptic responses to fear conditioning stimuli are similar in the LA and AStria.

(A) Heatmaps of monosynaptic responses in the LA showing z-scored PSTHs for CS (left), US (middle), and CS+US (right) stimuli. Only neurons with detected responses in the monosynaptic window (0-25ms post-stimulus) are shown, sorted by cluster (CS-selective, US-selective, Multisensory). Color scale shows z-score normalized to baseline. Black lines separate clusters. **(B)** Firing rate (FR, Hz) bar charts comparing CS, US, and CS+US responses for each LA cluster. Stacked vertically: CS-selective (top), US-selective (middle), Multisensory (bottom). Bars show mean ± SEM. Statistical comparisons use Wilcoxon signed-rank test (*p<0.05, **p<0.01, ***p<0.001). **(C)** Heatmaps of monosynaptic responses in the AStria, same format as panel A. **(D)** AStria firing rate (FR, Hz) bar charts, same format as panel B. **(E)** Pie charts showing similar proportions of CS-selective, US-selective, and Multisensory neurons among monosynaptic responders in the LA (left) and AStria (right). Percentages indicate fraction of monosynaptic neurons in each category. **(F)** Across region comparison of firing rate (FR, Hz) for CS (left), US (middle), and CS+US (right) monosynaptic responders comparing LA vs AStria neurons. Individual data points shown as grey circles with jitter. Bars show mean ± SEM. Statistical comparison using Wilcoxon rank-sum test (*p<0.05, **p<0.01, ***p<0.001, n.s.=not significant). Y-axis scaled to 95th percentile to avoid compression from outliers. **(G)** Onset latency comparison for monosynaptic responses. Three panels show CS, US, and CS+US

onset latencies (ms) comparing LA vs AStria neurons. Bars show mean ± SEM. Statistical comparison using Wilcoxon rank-sum test (*p<0.05, **p<0.01, ***p<0.001, n.s.=not significant).

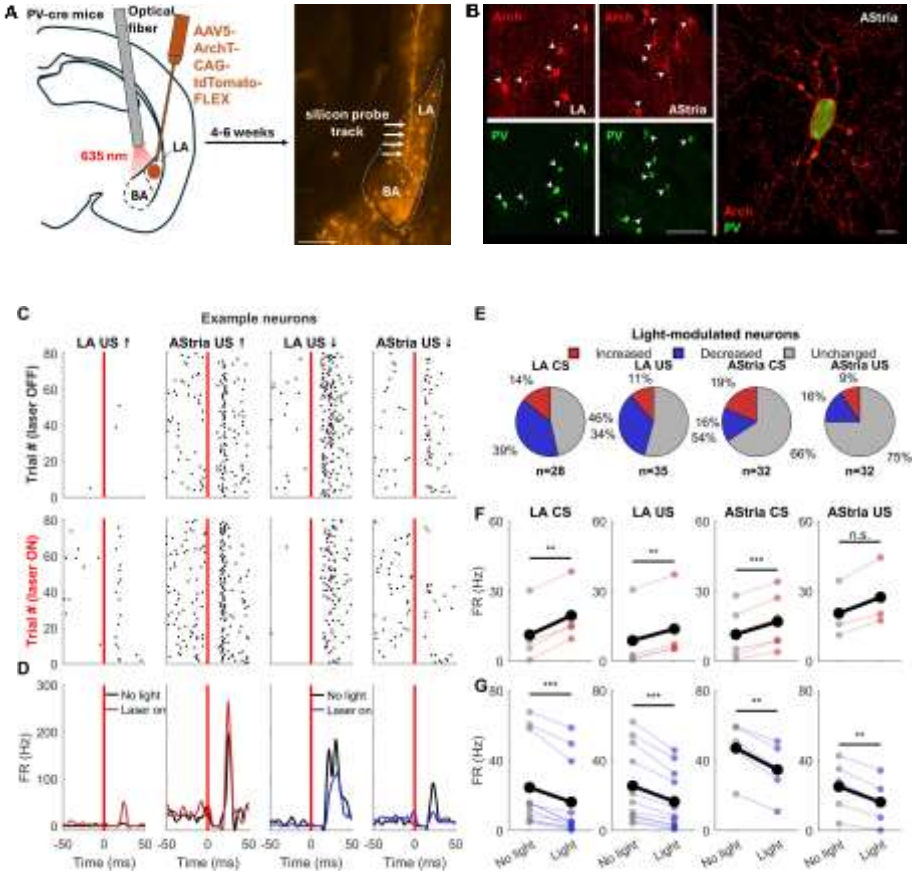

Figure 5: A fraction of monosynaptic responses in the LA and AStria are controlled by PV interneurons.

(A) Left: Schematic of stereotaxic injections in PV-Cre mice. AAV5-ArchT-CAG-tdTomato-FLEX virus was delivered into the LA and AStria, followed by implantation of an optical fiber positioned above the LA for 635-nm light delivery to inhibit PV-expressing interneurons. Following 4–6 weeks of viral expression, a silicon probe was inserted to record neural activity during optogenetic manipulation.Right: Representative fluorescence image showing tdTomato-expressing neurons in the BA and LA, along with the track of the silicon probe (arrows). Dashed lines outline the anatomical boundaries of the LA and BA. **(B)** Left: Micrographs showing Arch-expression (top) in PV-positive neurons (bottom) in the LA and AStria. Right: Individual, PV-positive Astria neuron expresses

Arch throughout the membrane. Scale bars: left, 100 μm; right, 10 μm. **(C)** Example raster plots showing individual neuron responses to CS or US stimuli without light (top row) and with light (middle row) for four example neurons. Each row represents one trial, with spike times shown as vertical marks. Red vertical line indicates stimulus onset. **(D)** Lines for the same example neurons showing average firing rate (Hz) over time for no-light (black) and light (red) conditions. Time axis centered at stimulus onset (0 ms). Each plot shows the peristimulus time histogram comparing baseline and optogenetic manipulation conditions. **(E)** Pie charts showing proportions of neurons with enhanced, decreased, and unchanged monosynaptic responses during inhibiting PV interneurons. Numbers and percentages indicate fraction of responsive neurons in each category. **(F)** Plots showing trial-averaged spike counts for individual enhanced neurons comparing no-light (left, black) vs light (right, red) conditions. Each gray line represents one neuron, with population mean shown in bold. Four panels correspond to LA CS, LA US, AStria CS, and AStria US enhanced neurons. Enhancement detected using Wilcoxon signed-rank test ($p<0.05$) comparing spike counts in the monosynaptic window (12-50 ms) between light and no-light conditions. **(G)** Plots showing trial-averaged spike counts for individual decreased neurons comparing no-light vs light conditions, formatted as in panel F. Decreased responses were identified using the same statistical criteria.

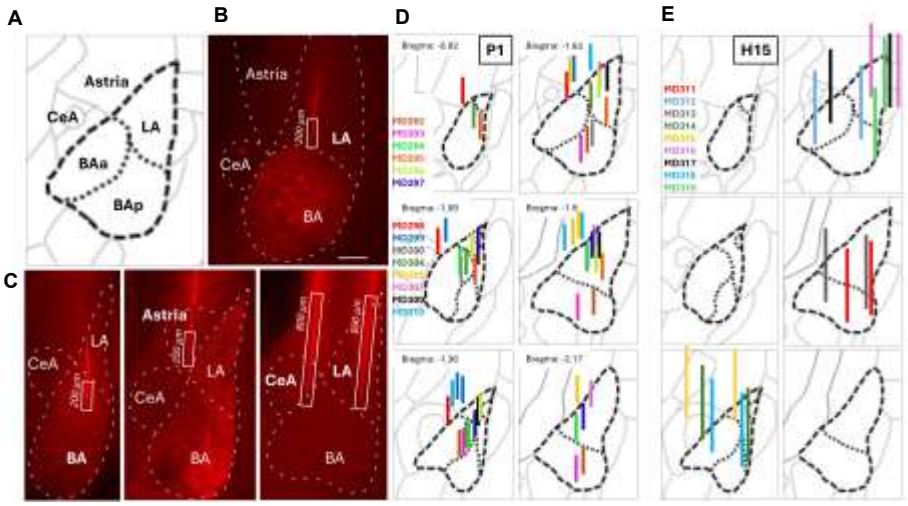

Supplementary Figure 1: Position of electrode tracks in the BLA, CeA and Astria. **(A)** Schematic map of the BLA, CeA and Astria. **(B)** Recording electrode tracks in LA. White boxes indicate the distribution of recording sites in inhibitory opsin (Archeorhodopsin) -injected tissue. **(C)** Example images of recording sites in BA/LA (left), Astria (middle) and CeA/LA (right) recordings. **(D)** Schematics present the distribution of recording electrodes in different experiments (each color represents a distinct animal) using the P1 probe (4 shanks, 200 µm of recording sites on tip). **(E)** as in (D) using the H15 probe (2 shanks, 800 µm of recording sites on tip). Scale: 200 µm

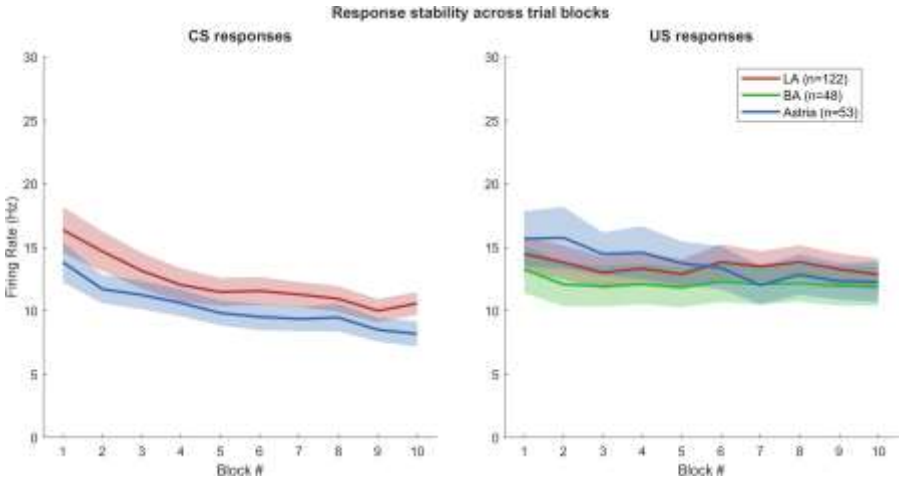

Supplementary Figure 2. Stability of neuronal responses across trial blocks.
Block-averaged firing rates (mean ± SEM; 5 trials per block) for neurons responsive to the CS (left) and US (right) in the LA (red), BA (green), and Astria (blue). Responses were averaged across neurons classified as responsive (CS-selective/Multisensory for CS; US-selective/Multisensory for US) and plotted over the 50 trials (10 blocks). Shaded areas represent SEM. Data corresponds to Table 2.

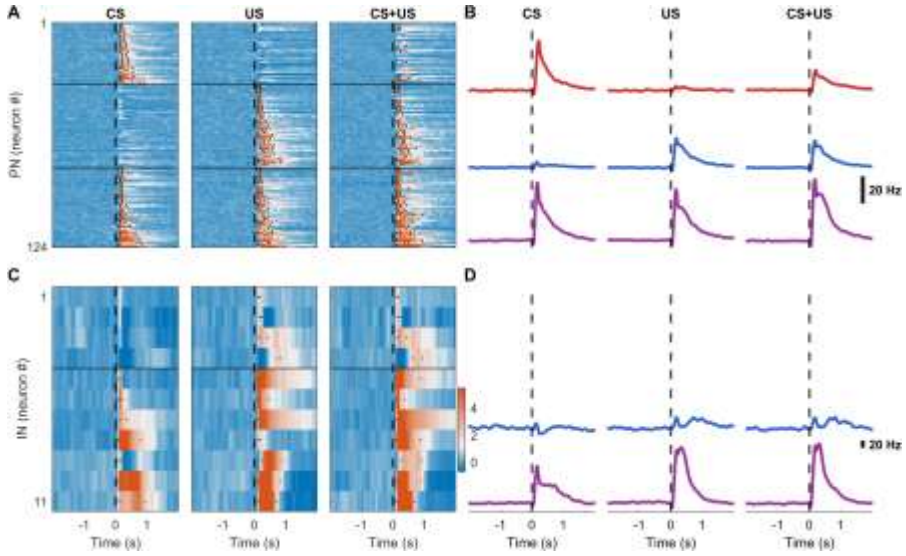

Supplementary Figure 3 - PN vs IN: Cell type comparison of response profiles in the lateral amygdala.

(A) PN (principal neuron) heatmaps showing z-scored PSTHs for CS (left), US (middle), and CS+US (right) stimuli in the LA. Neurons sorted by cluster (CS-selective, US-selective, Multisensory, non-responsive, inhibited) based on CS and US responses only. Color scale shows z-score normalized to baseline. Black lines separate clusters. **(B)** Lines showing population average firing rates (Hz) for CS-selective (red), US-selective (blue), and Multisensory (purple) neurons. Each cluster displayed separately (stacked rows) for CS, US, and CS+US stimuli. Scale bar: 20 Hz. **(C)** IN (interneuron) heatmaps, same format as panel A. **(D)** Lines, same format as panel B.

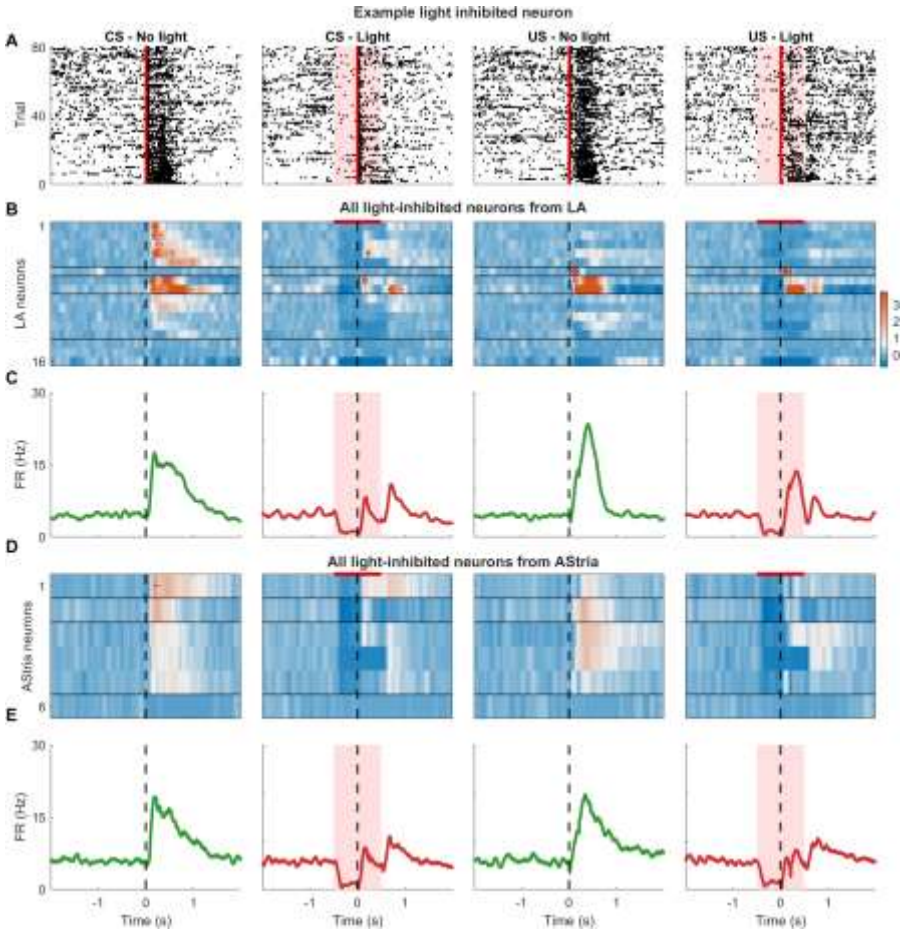

Supplementary Figure 4: Light-inhibited PV interneurons during optogenetic manipulation.

(A) Example raster plots from a single light-inhibited neuron recorded in PV-Cre mice injected with AAV5-CAG-FLEX-ArchT-tdTomato showing responses to CS and US stimuli. Four columns show CS no-light, CS light, US no-light, and US light conditions. Each row represents one trial with spike times shown as vertical marks. Red vertical line indicates stimulus onset. **(B)** Heatmaps of LA PV interneurons showing z-scored PSTHs for all light-inhibited neurons sorted by stimulus preference. Four panels show CS no-light, CS light, US no-light, and US light conditions. Color scale shows z-score normalized to

baseline. PV interneurons sorted to maximize similarity in response patterns. **(C)** Lines shown average firing rate for light-inhibited neurons. Four panels show mean firing rate (Hz) over time for CS no-light (black), CS light (red), US no-light (black), and US light (red) conditions. Time axis centered at stimulus onset (0 ms). Shaded areas represent SEM. **(D)** Heatmaps of AStria PV interneurons showing z-scored PSTHs for all light-inhibited neurons, same format as panel B. **(E)** Lines show average firing rate for light-inhibited PV interneurons, same format as panel C. Light-inhibited neurons identified using Wilcoxon rank sum test comparing recent baseline (−0.5 to 0s) vs earlier baseline (−5 to −0.5s) with criterion of $p<0.05$ and ≥50% firing rate drop.